

**This is the accepted manuscript (postprint) of the following article:**

Majid Hosseinzadeh, Erfan Salahinejad, *Influence of Pt/Ru ratios on the oxidation mechanism of MCrAlYTa coatings modified with PtRu overlays*, Surface and Coatings Technology, 510 (2025) 132224.

<https://doi.org/10.1016/j.surfcoat.2025.132224>

# **Influence of Pt/Ru ratios on the oxidation mechanism of MCrAlYTa coatings modified with Pt-Ru overlays**

Majid Hosseinzadeh, Erfan Salahinejad\*

*Faculty of Materials Science and Engineering, K.N. Toosi University of Technology, Tehran, Iran*

\* Corresponding Author's Email Address: <salahinejad@kntu.ac.ir>

## **Abstract**

This study investigates the influence of varying Pt/Ru ratios on the oxidation mechanism of NiCoCrAlYTa coatings with electrodeposited, vacuum-annealed Pt-Ru overlays. Weight change measurements, scanning electron microscopy/energy dispersive X-ray spectrometry (SEM/EDS), X-ray diffraction (XRD), and X-ray photoelectron spectroscopy (XPS) were used for high-temperature oxidation analyses, showing superior resistance with higher Pt contents. This was attributed to the creation of a denser, thinner, and more homogeneous layer of alumina ( $\alpha$ -Al<sub>2</sub>O<sub>3</sub>) in the thermally-grown oxide (TGO) layer. On the contrary, an increase in Ru contents led to the development of other oxides and microcracks along with alumina in the TGO layer, undermining oxidation protection. The accommodation of Ti and Ta, in the minimally-deteriorative form of carbide, along with Y into the TGO layer with increasing Pt contents further enhanced oxidation resistance. In addition to the explored significant impact of the Pt/Ru ratio on oxide scale characteristics and oxidation resistance, the lower cost of Ru compared to Pt suggests the potential for designing cost-effective systems through optimized Pt/Ru ratios and microstructural engineering.

**Keywords:** Thermal-barrier coating (TBC); Interdiffusion, Enthalpy of mixing; Spinel oxides

**This is the accepted manuscript (postprint) of the following article:**

Majid Hosseinzadeh, Erfan Salahinejad, *Influence of Pt/Ru ratios on the oxidation mechanism of MCrAlYTa coatings modified with PtRu overlays*, Surface and Coatings Technology, 510 (2025) 132224.

<https://doi.org/10.1016/j.surfcoat.2025.132224>

## 1. Introduction

MCrAlY (with M representing Ni and/or Co) coatings are commonly utilized within thermal-barrier coatings (TBCs) on hot-section components in aerospace and terrestrial gas turbine engines to offer high-temperature oxidation and corrosion resistance. The superior efficacy of this protective layer, used as either an overlay or a bond coat, is mainly ascribed to the development of a dense, adherent, stable, slowly growing, and continuous alumina ( $\alpha$ -Al<sub>2</sub>O<sub>3</sub>) layer on the surface, called thermally-grown oxide (TGO). The longevity of MCrAlY coatings is predominantly influenced by the extent of aluminum consumption within the coating, driven by surface oxidation and diffusion into the underlying substrate. Additionally, issues like cracking, rumpling, and spallation at the TGO scale culminate in TBC degradation [1, 2]. These challenges highlight the necessity of modifying traditional MCrAlY coatings to enhance the system's lifetime and reliability.

The ability of MCrAlY coatings to resist oxidation can be enhanced through several mechanisms: 1) enhancing TGO layer adhesion to the coating surface to prevent spallation, 2) reducing the TGO growth rate to delay attaining the critical thickness, and 3) minimizing the reciprocal diffusion of the alloy constituents between the coating and substrate [3]. A well-documented and effective method for modifying these coatings is the incorporation of platinum (Pt). The advantageous impacts of Pt additions on MCrAlY coatings encompass: (1) reducing growth stress within the oxide scale [4, 5], (2) enhancing aluminum affinity and facilitating its uphill diffusion [6, 7], (3) inhibiting void formation beneath the oxide scale [8, 9], (4) promoting outward aluminum diffusion while restricting the diffusion of alloying elements, thereby reducing the development of non-protective oxides and supporting the creation of a pure alumina layer [10, 11], and (5) promoting alumina formation and enhancing alumina layer adhesion [12, 13]. However, Pt-modified coatings are susceptible to rumpling in the course of

**This is the accepted manuscript (postprint) of the following article:**

Majid Hosseinzadeh, Erfan Salahinejad, *Influence of Pt/Ru ratios on the oxidation mechanism of MCrAlYTa coatings modified with PtRu overlays*, Surface and Coatings Technology, 510 (2025) 132224.

<https://doi.org/10.1016/j.surfcoat.2025.132224>

thermal cycling owing to the mismatch in thermal expansion coefficients between TGO and its underlying coating. This phenomenon results in the considerable out-of-plane displacement of TGO, which can initiate cracks within or between the multilayers of the TBC system, ultimately giving rise to the spallation of the TBC [14, 15]. Also, the high cost of Pt remains a barrier for its widespread application, driving research into partial or complete alternatives that provide comparable outcomes.

Ruthenium (Ru) incorporation is a viable option for enhancing the high-temperature performance of bond coats, where Ru offers chemical properties similar to Pt at a more cost-effective price while reducing rumpling. These enhancements are attributed to: 1) promoting the formation of transient alumina [16, 17], 2) forming thinner  $\alpha$ -Al<sub>2</sub>O<sub>3</sub> scales [18, 19], 3) decreases the Al activity, which slows the growth rate of alumina [20], and 4) increasing the creep and rumpling resistance of the bond coat [21, 22]. A recent preliminary study by the same authors provided observations on the oxidation protection of pure Ru, pure Pt, and a Pt-Ru alloy (66Pt-34Ru in wt%) overlays on an MCrAlY bond coat [23], without exploring a broader range of Pt/Ru ratios or presenting a more comprehensive analysis of the involved mechanisms. The present work systematically examines a broader range of Pt/Ru ratios, particularly compositions across distinct regions of the Pt-Ru phase diagram [24], including a Pt-rich solid solution, a Ru-rich solid solution, and a biphasic composition of Pt and Ru. By providing insights into the potential of these additives, both individually and in combination, this study aims to explore possible synergistic effects and inform the design of more efficient and cost-effective bond coats with enhanced oxidation protection.

## **2. Experimental procedure**

### ***2.1. Sample preparation***

**This is the accepted manuscript (postprint) of the following article:**

Majid Hosseinzadeh, Erfan Salahinejad, *Influence of Pt/Ru ratios on the oxidation mechanism of MCrAlYTa coatings modified with PtRu overlays*, Surface and Coatings Technology, 510 (2025) 132224.

<https://doi.org/10.1016/j.surfcoat.2025.132224>

NiCoCrAlYTa powder (Amdry 997, Sulzer Metco), with a mean particle size of approximately 30  $\mu\text{m}$ , was employed as the coating material for grit-blasted CMSX-4 superalloy specimens, applied via a high-velocity oxygen-fuel (HVOF) spraying apparatus (GTV Verschleiss- Schutz GmbH, Germany). Table 1 lists the nominal composition of the CMSX-4 superalloy and NiCoCrAlYTa powder used in this study. The operational parameters for HVOF deposition are also tabulated in Table 2.

**Table 1.** Chemical composition of the CMSX-4 superalloy and the Amdry997 powder (wt%)

	Ni	Co	Cr	Al	Y	Ta	Ti	W	Mo	Re	Hf
CMSX-4	54.5	9.5	6.4	5.7	6.5	6.5	1.0	6.3	0.6	2.9	0.1
Amdry997	43.9	23.0	20.0	8.5	0.6	4.0	-	-	-	-	-

**Table 2.** HVOF parameters used for depositing NiCoCrAlYTa on the CMSX-4 substrate

Parameters	Value
Oxygen flow rate (standard liter per minute, SLPM)	850
Kerosene flow rate (SLPM)	0.5
Carrier gas (Ar) flow rate (SLPM)	7
Spraying distance (mm)	300
Powder feed rate (g/min)	90
Spray gun traversing velocity (mm/s)	3

The electrodeposition procedure of Pt on the NiCoCrAlYTa-coated samples was performed in an alkaline solution containing  $\text{Pt}(\text{NH}_3)_2(\text{NO}_2)_2$  at 90 °C, with a platinum level of 10 g/L, pH of 11, and the current density of 1 A/dm<sup>2</sup> for 180 min. The electrodeposition process for Ru was executed within a solution containing  $\text{RuCl}_3$  at 70 °C, demonstrating a substantial Ru concentration of 5 g/L and pH of 1, at a current density of 5 A/dm<sup>2</sup> for 60 min. The electrodeposition bath for the Pt/Ru alloy also comprised stoichiometrically balanced

**This is the accepted manuscript (postprint) of the following article:**

Majid Hosseinzadeh, Erfan Salahinejad, *Influence of Pt/Ru ratios on the oxidation mechanism of MCrAlYTa coatings modified with PtRu overlays*, Surface and Coatings Technology, 510 (2025) 132224.

<https://doi.org/10.1016/j.surfcoat.2025.132224>

concentrations of  $\text{Pt}(\text{NH}_3)_2(\text{NO}_2)_2$  and  $\text{RuCl}_3$ , specifically 5-10 g/L of the former and 5 g/L of the latter at the current densities of 2, 3, and 4  $\text{A}/\text{dm}^2$  for 90 min, for the nominal compositions of 70Pt-30Ru, 30Pt-70Ru and 10Pt-90Ru in wt%, respectively, at pH of 3. Then, the specimens underwent vacuum annealing at 1080 °C for 6 h. Figure 1 illustrates a detailed overview of the different coated samples and manufacturing processes used.

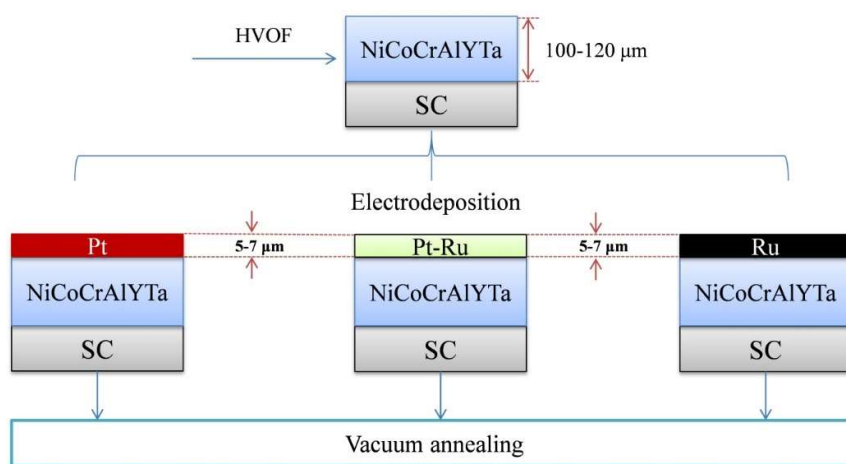


**Figure 1.** Schematic illustration of the preparation process (SC stands for single-crystal CMSX4 superalloy).

## 2.2. Structural characterization

The top and cross-sectional morphologies of the samples were systematically analyzed utilizing field-emission electron microscopy (FESEM, TESCAN, MIRA3) in both secondary electron (SE) and backscattered electron (BSE) imaging modes, which was complemented by energy dispersive X-ray spectrometry (EDS).

## 2.3. High-temperature oxidation characterization

Isothermal oxidation experiments were performed in a muffle furnace at 1100 °C for a duration of up to 200 h in air. Variations in the mass of the specimens were recorded at consistent intervals utilizing an A&D analytical balance, across three separate trials. X-ray

**This is the accepted manuscript (postprint) of the following article:**

Majid Hosseinzadeh, Erfan Salahinejad, *Influence of Pt/Ru ratios on the oxidation mechanism of MCrAlYTa coatings modified with PtRu overlays*, Surface and Coatings Technology, 510 (2025) 132224.

<https://doi.org/10.1016/j.surfcoat.2025.132224>

diffraction (XRD, EXPLORER, GNR) utilizing Cu K $\alpha$  radiation was also utilized to characterize the phase structures formed in the samples during the oxidation tests, while the obtained morphologies and compositions were analyzed by SEM-EDS. Additionally, X-ray photoelectron spectroscopy (XPS, Bestek) was conducted using monochromatic aluminum K-alpha excitation (1486.7 eV) at an operating power of 108 W to evaluate the surface chemistry of the samples. The XPS spectra were also calibrated using carbon correction, in agreement with Refs. [25, 26].

### **3. Results**

#### ***3.1. Structural analysis of the electrodeposited overlay coatings***

The top-view SE microstructures and EDS spectra of the as-electrodeposited coatings are revealed in Figure 2. The coatings exhibit complete coverage and relatively uniform morphological features, while the EDS profiles indicate only peaks corresponding to Pt and Ru. The EDS-extracted chemical compositions of the nominal Pt, 70Pt-30Ru, 30Pt-70Ru, 10Pt-90Ru, and Ru coatings were 99.4Pt, 71.3Pt-27.6Ru, 31.6Pt-67.8Ru, 11.4-Pt 88.1Ru, and 99.2Ru (in wt%), respectively.

This is the accepted manuscript (postprint) of the following article:

Majid Hosseinzadeh, Erfan Salahinejad, *Influence of Pt/Ru ratios on the oxidation mechanism of MCrAlYTa coatings modified with PtRu overlays*, Surface and Coatings Technology, 510 (2025) 132224.

<https://doi.org/10.1016/j.surfcoat.2025.132224>

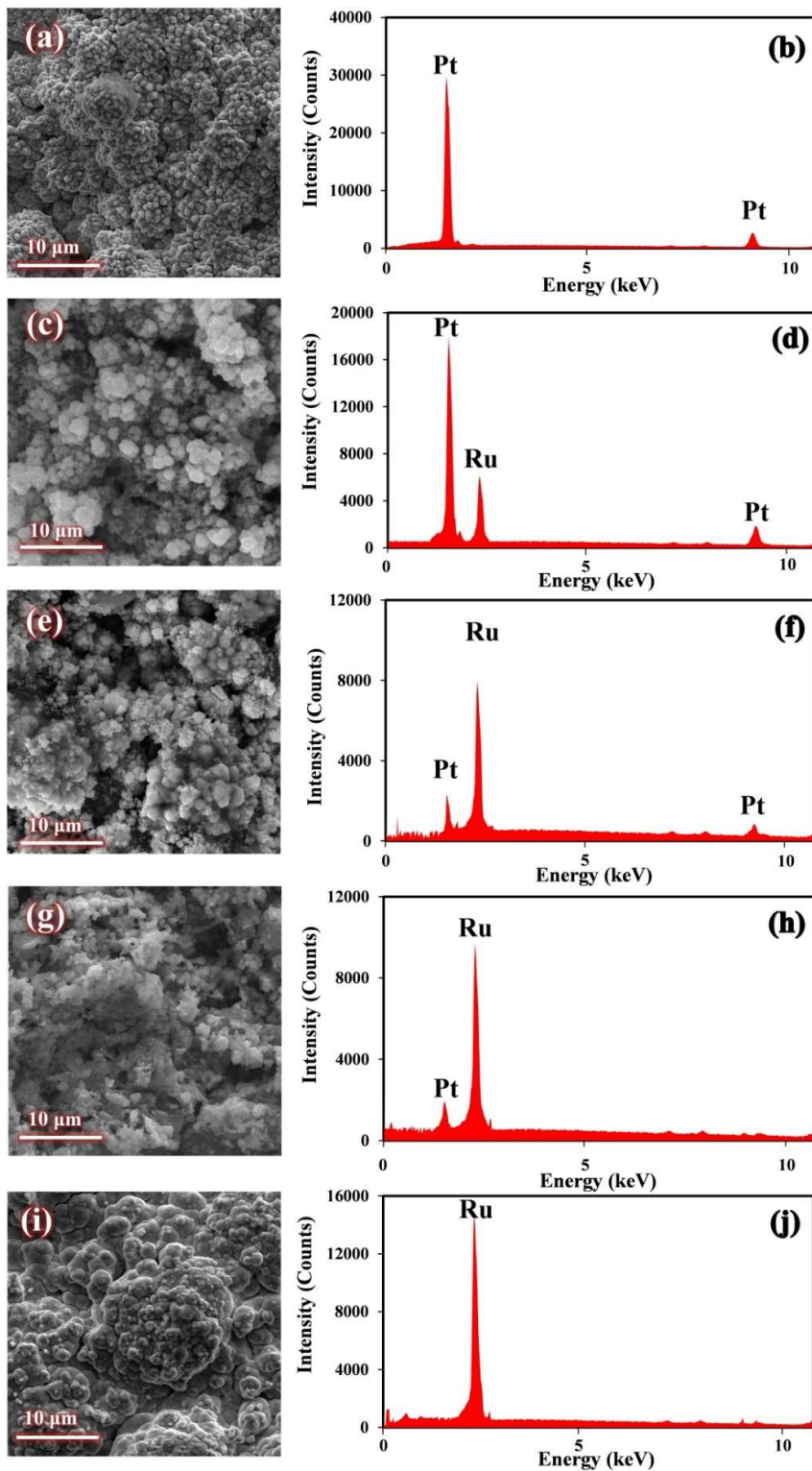


**Figure 2.** SE surface images and EDS profiles of the as-electrodeposited Pt (a, b), 70Pt-30Ru (c, d),

30Pt-70Ru (e, f), 10Pt-90Ru (g, h), and Ru (i, j) coatings.

**This is the accepted manuscript (postprint) of the following article:**

Majid Hosseinzadeh, Erfan Salahinejad, *Influence of Pt/Ru ratios on the oxidation mechanism of MCrAlYTa coatings modified with PtRu overlays*, Surface and Coatings Technology, 510 (2025) 132224.

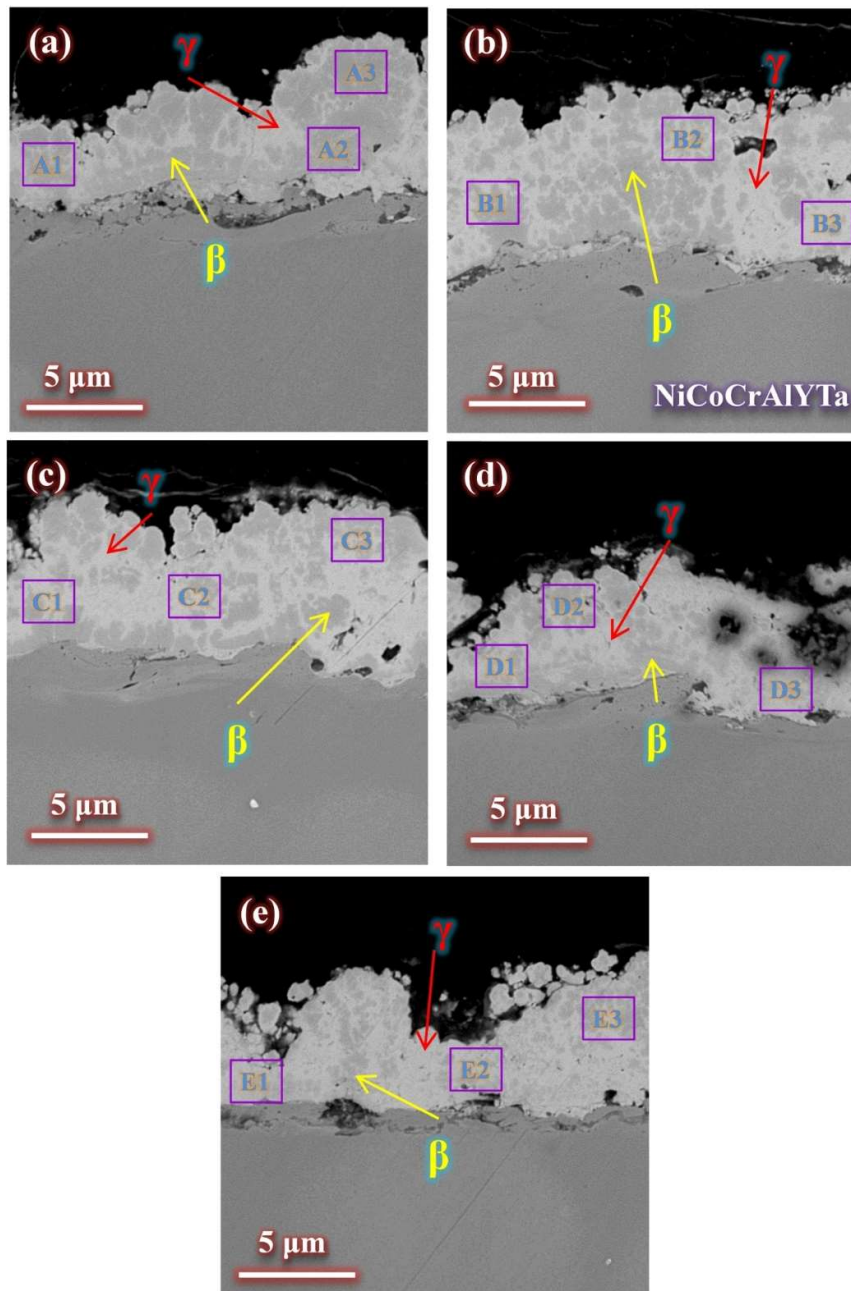
<https://doi.org/10.1016/j.surfcoat.2025.132224>

Figure 3 represents the cross-sectional BSE micrographs of the electrodeposited, annealed samples. After annealing at 1080 °C for 6 h, the Pt, Ru, and Pt-Ru layers exhibit two distinct contrasts assigned to  $\gamma$  and  $\beta$  phases, serving as the matrix and discontinuous dispersions, respectively. As observed, the proportion of the  $\beta$  phase decreases slightly with increasing the Ru content in the overlays. Table 3 tabulates the EDS-determined compositions (mean  $\pm$  standard deviation) of the areas marked in Figure 3. The data indicate that the level of Ni in the Pt layer is higher compared to all the Ru-containing layers, but with no significant variations observed among the Ru-containing overlays. The levels of Co and Cr exhibit no consistent dependency on the composition of the electrodeposited layers. However, an increase in the Ru content corresponds to a progressive reduction in the Al content of the overlays, while the concentrations of Y, Ta, and Ti show a gradual increase.

This is the accepted manuscript (postprint) of the following article:

Majid Hosseinzadeh, Erfan Salahinejad, *Influence of Pt/Ru ratios on the oxidation mechanism of MCrAlYTa coatings modified with PtRu overlays*, Surface and Coatings Technology, 510 (2025) 132224.

<https://doi.org/10.1016/j.surfcoat.2025.132224>



**Figure 3.** Cross-sectional BSE-SEM images for the Pt (a), 70Pt-30Ru (b), 30Pt-70Ru (c), 10Pt-90Ru (d), and Ru (e) deposited samples after annealing at 1080 °C for 6 h.

**Table 3.** EDS-extracted compositions of the areas indicated in Figure 3, taken from three different regions for each sample

Location	Content (wt%)
----------	---------------

This is the accepted manuscript (postprint) of the following article:

Majid Hosseinzadeh, Erfan Salahinejad, *Influence of Pt/Ru ratios on the oxidation mechanism of MCrAlYTa coatings modified with PtRu overlays*, Surface and Coatings Technology, 510 (2025) 132224.

<https://doi.org/10.1016/j.surfcoat.2025.132224>

	Pt	Ru	Ni	Co	Cr	Al	Y	Ta	Ti
A	30.2±2.5	0.0	25.6±1.5	11.1±0.5	8.4±0.6	23.4±2.0	0.0	0.2±0.1	0.3±0.1
B	21.3±1.5	11.4±1.5	21.4±2.1	13.4±1.1	11.2±0.5	19.6±1.5	0.0	0.8±0.5	0.3±0.1
C	11.5±0.5	24.1±1.5	20.1±1.8	12.2±1.1	11.5±0.8	18.2±1.5	0.2±0.1	1.8±0.1	0.3±0.1
D	5.2±0.1	31.3±2.5	23.2±2.1	11.3±1.1	9.4±0.6	16.2±1.2	0.3±0.1	2.5±0.1	0.4±0.1
E	0.0	37.4±2.2	21.5±1.5	12.2±1.1	10.4±0.9	14.2±1.2	0.5±0.1	3.2±0.5	0.5±0.1

### 3.2. Oxidation behavior of the samples

Figure 4 indicates the oxidation kinetic curves of the specimens at 1100 °C. The results depict that the oxidation resistance follows the order: Pt-coated > 70Pt-30Ru-coated > 30Pt-70Ru-coated > 10Pt-90Ru-coated > Ru-coated >> bare NiCoCrAlYTa. In other words, while the electrodeposited coatings significantly enhance the oxidation resistance of the NiCoCrAlYTa-coated substrate, the protection slightly diminishes by increasing the Ru content.

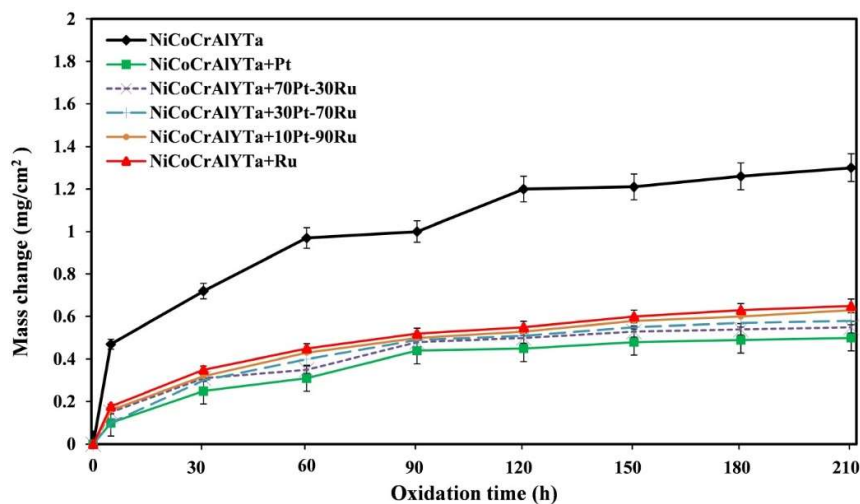


Figure 4. Oxidation weight change profile of the samples.

The XRD analysis was conducted on the surfaces after 50 and 200 h of isothermal oxidation (Figure 5). The NiCoCrAlYTa overlay sample exhibits  $\alpha$ -Al<sub>2</sub>O<sub>3</sub>, NiAl<sub>2</sub>O<sub>4</sub>,  $\gamma/\gamma'$ ,  $\alpha$ -Cr, and Cr<sub>2</sub>O<sub>3</sub> phases after 50 h of oxidation. By progression of oxidation to 200 h, diffraction

This is the accepted manuscript (postprint) of the following article:

Majid Hosseinzadeh, Erfan Salahinejad, *Influence of Pt/Ru ratios on the oxidation mechanism of MCrAlYTa coatings modified with PtRu overlays*, Surface and Coatings Technology, 510 (2025) 132224.

<https://doi.org/10.1016/j.surfcoat.2025.132224>

signals for the  $\alpha$ -Cr phase disappear, while signals for the other phases increase. For the Pt-Ru modified samples, the  $\alpha$ -Cr phase is absent and the oxides formed include  $\alpha$ -Al<sub>2</sub>O<sub>3</sub>, along with small amounts of spinel NiAl<sub>2</sub>O<sub>4</sub>. Extending the oxidation duration to 200 h results in a rise in both the intensity and number of the peaks. Over both test periods, the intensity and number of the NiAl<sub>2</sub>O<sub>4</sub> peaks show an increase, while those of the  $\alpha$ -Al<sub>2</sub>O<sub>3</sub> peaks decrease by increasing the Ru content of the electrodeposited coatings. Compared to the modified samples, the NiCoCrAlYTa overlay sample exhibits weaker  $\alpha$ -Al<sub>2</sub>O<sub>3</sub> signals but stronger spinel phase ones.

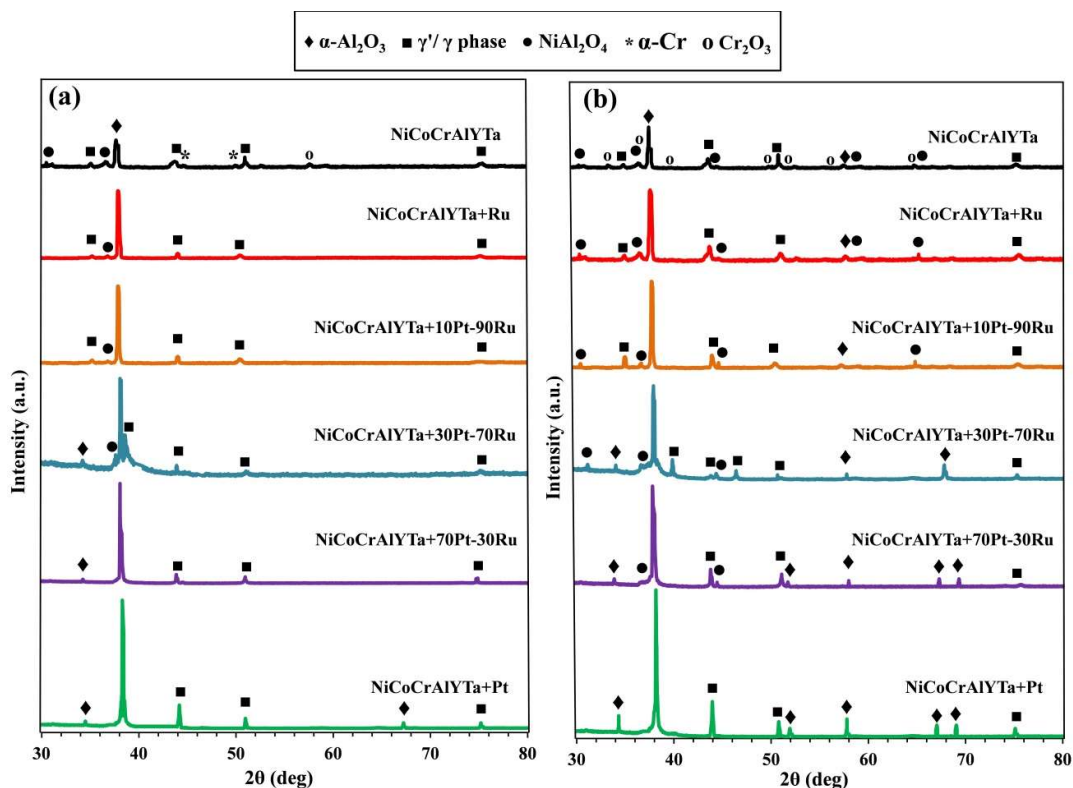


Figure 5. XRD profiles of the sample surfaces after oxidation exposure at 1100 °C for 50 (a) and 200 (b) h.

Figure 6 presents the top-view BSE-SEM observations of the Pt and Ru-modified samples after 200 h of oxidation, with the corresponding EDS analysis results summarized in Tables 4 and 5 for distinct locations identified in the micrographs. In the Pt-coated sample, the major phase is characterized to be rich in Al and O, corresponding to Al<sub>2</sub>O<sub>3</sub>, with traces of Ni,

**This is the accepted manuscript (postprint) of the following article:**

Majid Hosseinzadeh, Erfan Salahinejad, *Influence of Pt/Ru ratios on the oxidation mechanism of MCrAlYTa coatings modified with PtRu overlays*, Surface and Coatings Technology, 510 (2025) 132224.

<https://doi.org/10.1016/j.surfcoat.2025.132224>

Co, Cr, Y, Ta, and Ti. The microstructure also includes islands enriched in Pt and containing notable amounts of Ni and Al but entirely lacking Ta and Ti. Also, spallation zones and mixed oxides depleted of Ta and Ti are present but in minor quantities. In contrast, the Ru-coated sample exhibits a higher proportion of spallation zones, cracks, and mixed oxides, notably with the mixed oxides containing Ta and Ti.

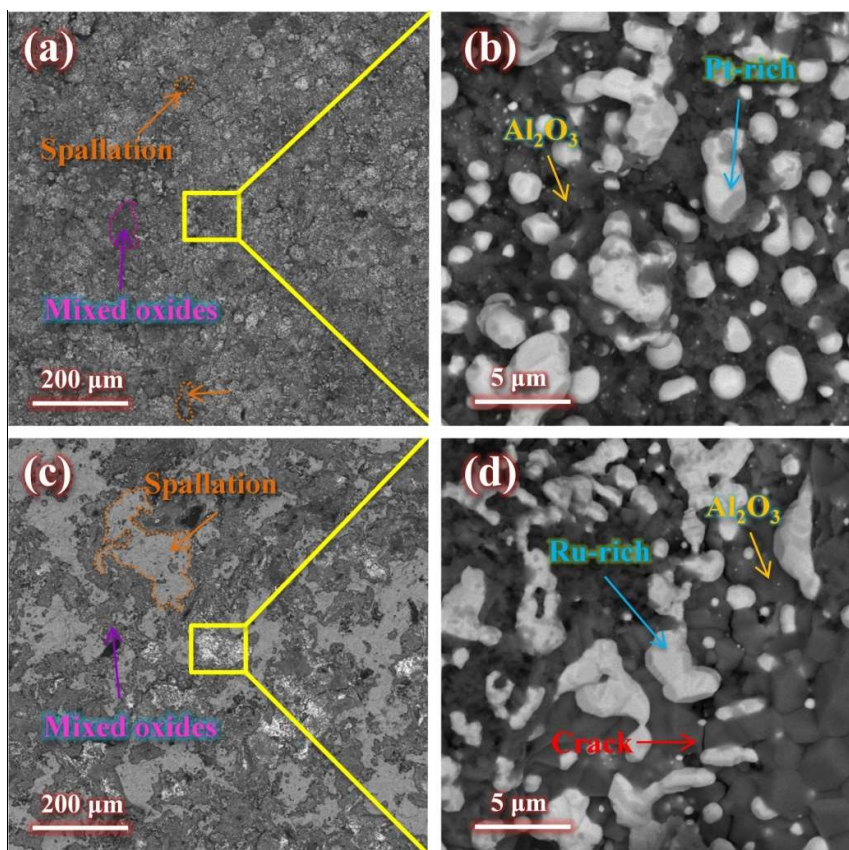


**Figure 6.** Surface BSE-SEM micrographs of the Pt- (a, b) and Ru (c, d)-modified samples after isothermal oxidation exposure at 1100 °C for 200 h.

**Table 4.** EDS composition of the regions marked in Figure 6 (a, b), based on three repetitions

Location	Content (wt%)									
	Pt	Ru	Ni	Co	Cr	Al	O	Y	Ta	Ti

**This is the accepted manuscript (postprint) of the following article:**

Majid Hosseinzadeh, Erfan Salahinejad, *Influence of Pt/Ru ratios on the oxidation mechanism of MCrAlYTa coatings modified with PtRu overlays*, Surface and Coatings Technology, 510 (2025) 132224.

<https://doi.org/10.1016/j.surfcoat.2025.132224>

<b>Mixed Oxides</b>	6.6±0.5	0.0	14.3±1.1	4.3±0.5	9.6±0.6	25.8±2.2	38.8±3.1	0.6±0.1	0.0	0.0
<b>Al<sub>2</sub>O<sub>3</sub></b>	0.0	0.0	1.2±0.1	1.4±0.1	2.6±0.1	33.8±3.1	54.8±5.1	0.2±0.1	4.7±0.1	1.3±0.1
<b>Pt-Rich</b>	45.8±3.5	0.0	27.3±2.5	4.1±0.1	5.3±0.2	13.2±1.1	3.6±0.1	0.7±0.1	0.0	0.0
<b>Spallation</b>	0.0	0.0	43.3±3.5	21.1±1.5	19.6±1.2	9.2±0.1	2.7±0.1	0.6±0.1	3.5±0.1	0.0

**Table 5.** EDS composition of the regions marked in Figure 6 (c, d), based on three repetitions

Location	Content (wt%)									
	Pt	Ru	Ni	Co	Cr	Al	O	Y	Ta	Ti
<b>Mixed Oxides</b>	0.0	9.8±0.1	26.1±2.1	4.2±0.1	4.1±0.1	19.2±1.5	29.5±2.5	3.4±0.1	3.5±0.1	0.2±0.1
<b>Al<sub>2</sub>O<sub>3</sub></b>	0.0	0.2±0.1	8.7±0.1	1.9±0.1	3.1±0.1	33.5±3.1	52.1±2.5	0.5±0.1	0.0	0.0
<b>Ru-Rich</b>	0.0	45.5±2.3	28.4±1.5	2.7±0.1	3.6±0.1	5.6±0.1	6.1±0.1	2.4±0.1	5.7±0.1	0.0
<b>Spallation</b>	0.0	0.0	41.4±2.6	22.6±1.3	21.3±1.1	8.4±0.1	1.6±0.1	0.5±0.1	4.2±0.1	0.0

The cross-sectional BSE-SEM micrographs and mapping of the Pt- and Ru-coated samples after isothermal oxidation at 1100 °C for 50 h are depicted in Figure 7, revealing four distinct contrasts. The bottom layer (A) corresponds to the NiCoCrAlYTa bond coat layer, which has undergone elemental interdiffusion with the upper layers. Layer B is predominantly composed of Al and O, while this layer in the Ru-coated sample is thicker and contains small dispersions of a secondary phase with a different contrast. In both samples, Layer C mainly consists of Ni, Co, Cr, Al, and O, while this layer in the Ru-coated sample contains Ti in contrast to the Pt-coated sample. The upper islands marked as D are rich in Pt or Ru and include traces of Ni, Co, and Cr. Notably, in the Pt-coated sample, the islands are mainly free of Ta, Ti, and Y but contains some Al, whereas in the Ru-coated sample, the islands are primarily free of Al and Ti but include a minor amount of Ta and Y.

This is the accepted manuscript (postprint) of the following article:

Majid Hosseinzadeh, Erfan Salahinejad, *Influence of Pt/Ru ratios on the oxidation mechanism of MCrAlYTa coatings modified with PtRu overlays*, Surface and Coatings Technology, 510 (2025) 132224.

<https://doi.org/10.1016/j.surfcoat.2025.132224>

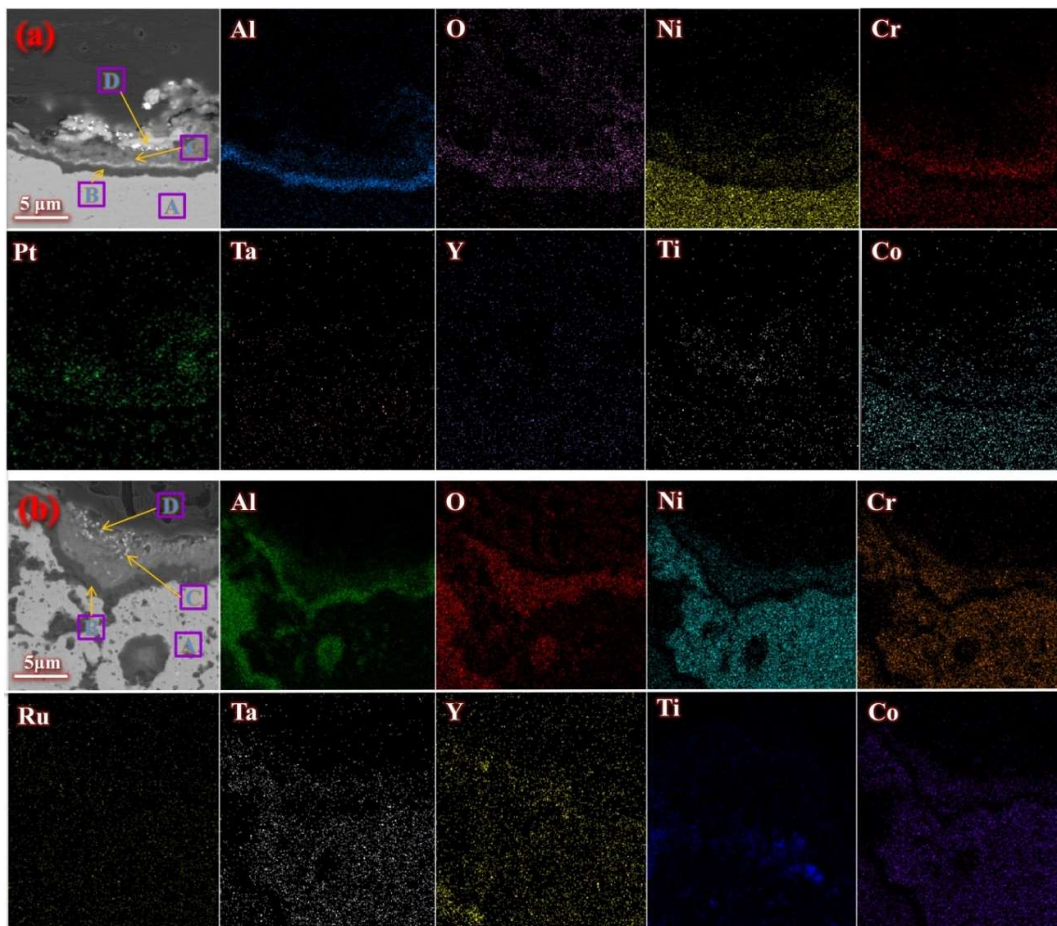


**Figure 7.** Cross-sectional BSE-SEM micrographs and maps for the Pt (a) and Ru (b) coated samples after oxidation at 1100 °C for 50 h.

Figure 8 demonstrates the effect of the Ru content in the electrodeposited overlays on the structural characteristics of the layers formed during oxidation. As observed, the increase of the Ru content leads to a progressive thickening and increased inhomogeneity of the  $\text{Al}_2\text{O}_3$  layer. In the Pt-coated sample, this layer contains small islands attributed to  $(\text{Ta}, \text{Ti})\text{C}$  [7, 27]. However, by increasing the Ru content, the  $\text{Al}_2\text{O}_3$  layer gradually incorporates an additional phase with a contrast distinct from the carbide observed in the Pt-coated sample, assigned to

This is the accepted manuscript (postprint) of the following article:

Majid Hosseinzadeh, Erfan Salahinejad, *Influence of Pt/Ru ratios on the oxidation mechanism of MCrAlYTa coatings modified with PtRu overlays*, Surface and Coatings Technology, 510 (2025) 132224.

<https://doi.org/10.1016/j.surfcoat.2025.132224>

other oxides, along with the development of microcracks. The dispersion of Pt-, Ru-, or Pt-Ru-rich islands within the mixed oxide matrix is also evident in these microstructures.

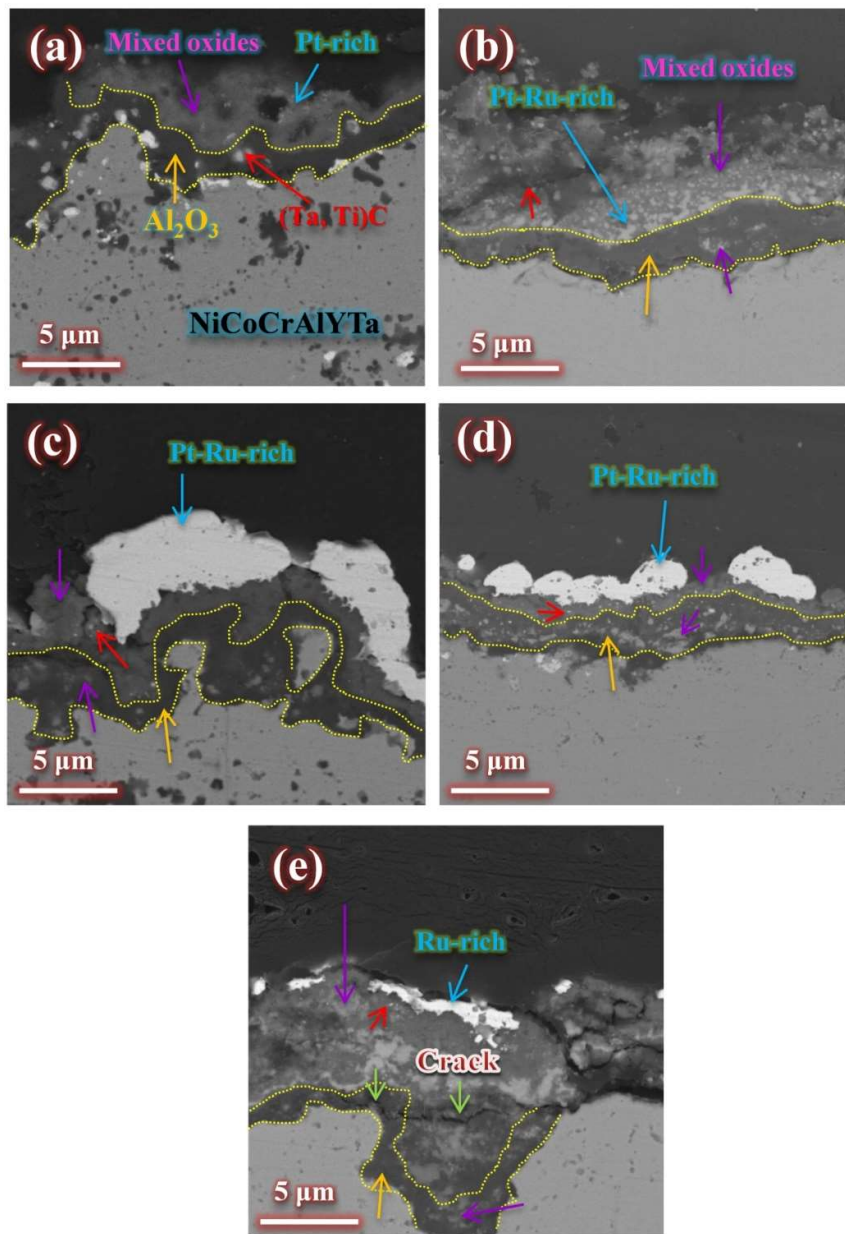


**Figure 8.** Cross-sectional BSE-SEM images of the Pt (a), 70Pt-30Ru (b), 30Pt-70Ru70 (c), 10Pt-90Ru90 (d), and Ru (e) coatings after oxidation at 1100 °C for 50 h.

**This is the accepted manuscript (postprint) of the following article:**

Majid Hosseinzadeh, Erfan Salahinejad, *Influence of Pt/Ru ratios on the oxidation mechanism of MCrAlYTa coatings modified with PtRu overlays*, Surface and Coatings Technology, 510 (2025) 132224.

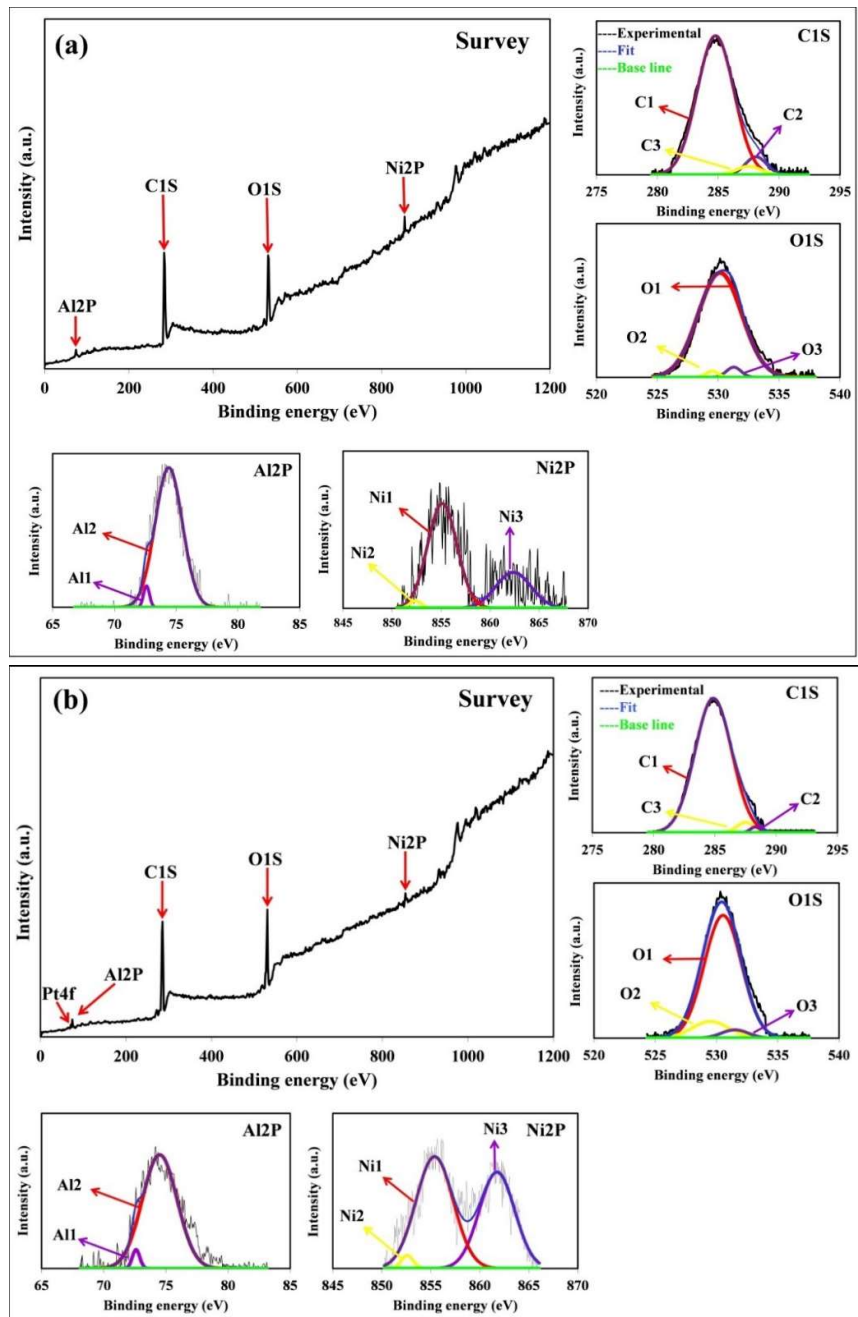
<https://doi.org/10.1016/j.surfcoat.2025.132224>

The XPS profiles of the sample surfaces after oxidation at 1100 °C for 200 h are revealed in Figure 9. For all the samples, the deconvolution of the high-resolution C 1s scan suggests the dominance of the C1 peak located at 284.9 eV, which can be assigned to C-C, C=C, and C-H bonds [28, 29]. Lower-intensity, higher-energy deconvoluted peaks, C2 and C3, correspond to C-O and C=O bonds, located at 286.3 and 288.3 eV, respectively [30, 31]. These detected bonds are representative of CO and CO<sub>2</sub> gases adsorbed during oxidation exposure [32]. The high-resolution scan of Al 2p for all the samples exhibits a broad band ranging from approximately 72 to 76 eV, structured by two primary peaks: Al1 at 72.6 eV and Al2 at 74.3 eV. The Al1 peak corresponds to the dominant Al 2p<sub>3/2</sub> component [33, 34], attributed to metallic Al within the  $\gamma'$  phase. The Al2 peak primarily represents the Al<sup>3+</sup> 2p<sub>3/2</sub> state and is associated with Al<sup>3+</sup> in Al<sub>2</sub>O<sub>3</sub>/NiAl<sub>2</sub>O<sub>4</sub> [35, 36]. The high-resolution fitting of the Ni 2p band indicates three peaks at 852.6 (Ni1), 855.1 (Ni2), and 862.2 (Ni3) eV, corresponding to Ni<sup>0</sup> 2p<sub>3/2</sub>, Ni<sup>2+</sup> 2p<sub>3/2</sub> and Ni satellite peaks, respectively, compatible with Refs. [37-41]. The peaks of Ni<sup>0</sup> and Ni<sup>2+</sup> are assigned to the  $\gamma'$  and NiAl<sub>2</sub>O<sub>4</sub> spinel phases, respectively. While Cr, Co, Y, and Ti were not detected on the surfaces, Ta was detected only in the Ru-coated sample. Specifically, the Ta<sup>0</sup> (Ta1), Ta<sup>5+</sup> 4f<sub>7/2</sub> (Ta2) and Ta<sup>4+</sup> 4f<sub>5/2</sub> (Ta3) peaks, centered at 21.9, 26.7, and 28.6 eV, correspond to metallic Ta, Ta<sub>2</sub>O<sub>5</sub> and TaO<sub>2</sub>, respectively [42-44] with the dominance of Ta<sub>2</sub>O<sub>5</sub>, realized from the relative intensity of the deconvoluted peaks. The O 1s envelope reflects the dominance of Al<sub>2</sub>O<sub>3</sub> species, corresponding to O<sup>2-</sup> at 530.7 eV, followed by NiAl<sub>2</sub>O<sub>4</sub> at 530.9 eV [40, 45, 46] in all the coatings. The O 1s peaks at 531.5 and 529.6 eV confirm the existence of Ta<sub>2</sub>O<sub>5</sub> and TaO<sub>2</sub>, respectively, aligning with Ref. [43, 47], in the NiCoCrAlYTa+Ru coating. Also, the peak of 531.5 eV is attributed to adsorbed oxygen species, including OH<sup>-</sup> in water and CO in CO<sub>3</sub><sup>2-</sup> [48].

This is the accepted manuscript (postprint) of the following article:

Majid Hosseinzadeh, Erfan Salahinejad, *Influence of Pt/Ru ratios on the oxidation mechanism of MCrAlYTa coatings modified with PtRu overlays*, Surface and Coatings Technology, 510 (2025) 132224.

<https://doi.org/10.1016/j.surfcoat.2025.132224>



This is the accepted manuscript (postprint) of the following article:

Majid Hosseinzadeh, Erfan Salahinejad, *Influence of Pt/Ru ratios on the oxidation mechanism of MCrAlYTa coatings modified with PtRu overlays*, Surface and Coatings Technology, 510 (2025) 132224.

<https://doi.org/10.1016/j.surfcoat.2025.132224>

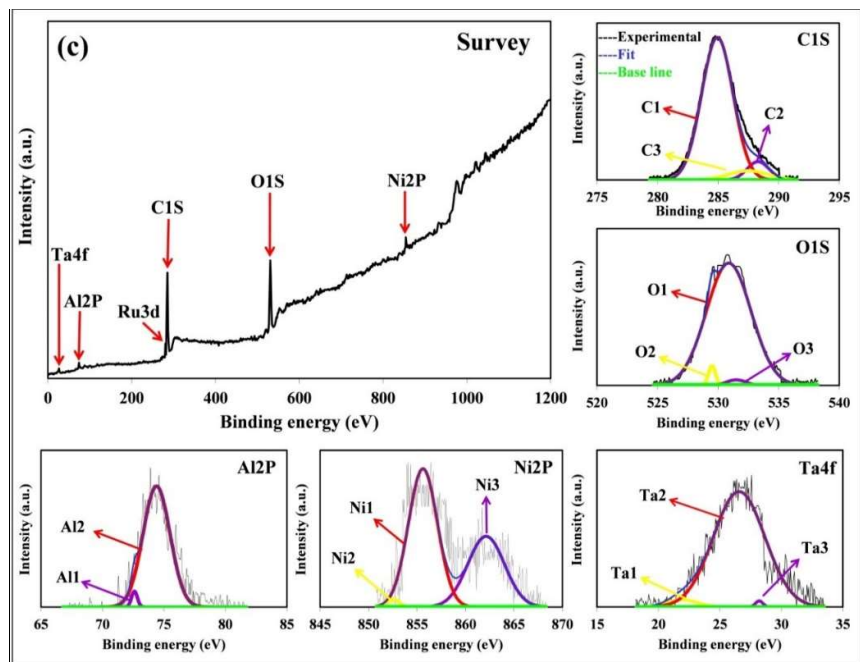


**Figure 9.** Survey and high-resolution XPS spectra for the NiCoCrAlYTa (a), NiCoCrAlYTa+Pt (b), and NiCoCrAlYTa+Ru (c) samples after oxidation at 1100 °C for 200 h.

## 4. Discussion

The exclusive observation of EDS peaks for Pt and Ru from the as-electrodeposited surfaces (Figure 2), with no detectable impurities, confirms the successful electrodeposition of these elements. Additionally, the uniform surface morphologies observed in Figure 2 further validate the controlled deposition process, achieved through the use of optimal bath chemistry and deposition parameters. According to our recent study [23], electrodeposited Pt, 66Pt-34Ru, and Ru overlays exhibited globular, dendritic, and cauliflower-like surface morphologies, respectively. These morphologies result from the interplay between charge-transfer and diffusion-controlled deposition mechanisms, which align with the findings in the present work from the uniformity viewpoint.

**This is the accepted manuscript (postprint) of the following article:**

Majid Hosseinzadeh, Erfan Salahinejad, *Influence of Pt/Ru ratios on the oxidation mechanism of MCrAlYTa coatings modified with PtRu overlays*, Surface and Coatings Technology, 510 (2025) 132224.

<https://doi.org/10.1016/j.surfcoat.2025.132224>

Vacuum-annealing of the electrodeposited samples facilitated the development of the  $\gamma$  and  $\beta$  phases within the overlays (Figure 3), which is consistent with findings reported in Refs. [5, 49, 50]. These phase structures are driven by the considerable interdiffusion of the elements from the HVOF-deposited NiCoCrAlYTa bond coat into the electrodeposited layers, as corroborated by the data in Table 3. Typically, the  $\gamma$  phase in the annealed Pt, Pt-Ru, and Ru overlays is a disordered FCC substitutional solid solution, with compositions based on Ni-Pt, Ni-Pt-Ru, and Ni-Ru, respectively. The  $\beta$  phase, richer in Al, is characterized by ordered B2-structured NiPtAl, NiPtRuAl, and NiRuAl intermetallic compounds, acting as a reservoir for Al for forming a protective Al<sub>2</sub>O<sub>3</sub> layer at elevated temperatures. The other elements listed in Table 3 are dissolved within these two phases [51-53] and/or form separate phases [5, 54], which are albeit difficult to distinguish due to their low quantities.

The variation observed in the compositions and relative phase levels observed in the annealed overlays (Table 3) can be explained by considering the sign and magnitude of the enthalpy of mixing between elemental pairs, which serves as a measure of their affinity [23, 55, 56]. The higher level of Ni diffusion into the pure Pt layer compared to the Ru-containing layers is attributed to the larger negative enthalpy of mixing between Pt and Ni (-5 kJ/mol) compared to Ru and Ni (0). However, the magnitude and difference in their enthalpy of mixing are not large enough to cause meaningful variations in the Ni concentration across the Ru-containing overlays. The irregular and insignificant dependency of the Co and Cr levels on the chemical composition of the electrodeposited layers can be also attributed to their low concentrations in the underlay and their relatively low affinity for the primary elements in the overlays. In contrast, Al exhibits a moderately exothermic enthalpy of mixing with both Pt and Ru, which facilitates its interdiffusion into the overlays. However, the lower concentrations of Al observed with increasing the Ru content are due to the stronger affinity of Pt for Al

**This is the accepted manuscript (postprint) of the following article:**

Majid Hosseinzadeh, Erfan Salahinejad, *Influence of Pt/Ru ratios on the oxidation mechanism of MCrAlYTa coatings modified with PtRu overlays*, Surface and Coatings Technology, 510 (2025) 132224.

<https://doi.org/10.1016/j.surfcoat.2025.132224>

compared to Ru, with enthalpies of mixing of -44 and -21 kJ/mol for Pt-Al and Ru-Al pairs, respectively. This results in a reduction of the  $\beta/\gamma$  ratio with an enhancement in the Ru content in the overlays, as Al—a primary constituent of the  $\beta$  phase—becomes less available, as seen in Figure 3. The accumulation trends of Y, Ta, and Ti can be attributed to their highly negative enthalpy of mixing with Pt, which inhibits their interdiffusion, and their moderately negative enthalpy of mixing with Ru, which facilitates their integration into the overlays.

A reciprocal connection of Figures 5-9 and Tables 4 and 5 highlights the microstructures formed during oxidation, thereby suggesting the associated oxidation mechanisms. During the oxidation process, the  $\beta$  phase shown in Figure 3 provides Al for the formation of  $\text{Al}_2\text{O}_3$  and other Al-containing oxides, detected by the XRD and XPS analyses in Figures 5 and 9, respectively. This phase is subsequently depleted of Al, and transforms into an ordered  $\text{L1}_2$ -structured substitutional solid solution ( $\gamma'$ ), with primary compositions of  $(\text{Ni, Pt})_3\text{Al}$ ,  $(\text{Ni, Pt, Ru})_3\text{Al}$ , and  $(\text{Ni, Ru})_3\text{Al}$  in the Pt, Pt-Ru, and Ru modified specimens, respectively, in agreement with Refs. [53, 57]. By progression of oxidation,  $\gamma'$  becomes depleted of Al and transforms into  $\gamma$ . As well as Al, other elements, including Ni, Co, and Cr, undergo oxidation, forming spinel phases, particularly  $\text{NiAl}_2\text{O}_4$  or  $(\text{Ni, Co, Cr})\text{Al}_2\text{O}_4$ , and/or other oxides like  $\text{NiCr}_2\text{O}_4$ , and  $\text{CoAl}_2\text{O}_4$  [50, 53]. Based on the XPS analysis (Figure 9),  $\text{NiAl}_2\text{O}_4$  is present in the surface layers, while the XRD (Figure 5) and EDS (Figures 6 and 7, and Tables 4 and 5) analyses showed the presence of mixed oxides in the subsurface layers. Accordingly,  $\gamma/\gamma'$  becomes enriched with Pt and Ru, as Pt and Ru are resistance to oxidation at 1100 °C [58], forming metallic islands rich in these noble elements, as indicated in Figures 6-9 and Tables 4 and 5, in agreement with Ref. [50, 59]. The appearance of  $\text{NiAl}_2\text{O}_4$  and/or  $(\text{Ni, Co, Cr})\text{Al}_2\text{O}_4$  in the XRD analysis (Figure 5) suggests the dominance of the spinel phase in the mixed oxide zones, assuming other oxides are also present. If distributed within a phase, Ta can trap Ti and

**This is the accepted manuscript (postprint) of the following article:**

Majid Hosseinzadeh, Erfan Salahinejad, *Influence of Pt/Ru ratios on the oxidation mechanism of MCrAlYTa coatings modified with PtRu overlays*, Surface and Coatings Technology, 510 (2025) 132224.

<https://doi.org/10.1016/j.surfcoat.2025.132224>

C diffusing from the superalloy toward the oxide scale through the formation of (Ta, Ti)C carbides [60, 61]; otherwise, Ti oxidation imposes detrimental effects on the overall oxidation resistance [54, 62].

A thorough comparison of the microstructures obtained in the various samples after oxidation (Figures 5-9 and Tables 3 and 4) can explain the observed oxidation mass gain and resistance (Figure 4), as schematically summarized in Figure 10. The most significant factor contributing to the enhanced oxidation resistance with increasing the Pt content is the evolution of the  $\alpha$ -Al<sub>2</sub>O<sub>3</sub> layer, which serves the primary component of oxidation protection in this system [7, 63]. As demonstrated in the XRD analysis (Figure 5), the relative amount of the  $\alpha$ -Al<sub>2</sub>O<sub>3</sub> phase is reduced by increasing the Ru content in the specimens, while the microscopic evaluations (Figures 6-8) reveal a deterioration in the compactness and homogeneity the Al<sub>2</sub>O<sub>3</sub> layer. This aligns well with the observed enhancement in Al accommodation and the  $\beta$  proportion with increasing the Pt content (Figure 3 and Table 3). Notably, the Al<sub>2</sub>O<sub>3</sub> layers in the samples coated with the Ru-containing overlays incorporate mixed oxides, which are well-documented to have a detrimental effect on oxidation [53, 64, 65].

This is the accepted manuscript (postprint) of the following article:

Majid Hosseinzadeh, Erfan Salahinejad, *Influence of Pt/Ru ratios on the oxidation mechanism of MCrAlYTa coatings modified with PtRu overlays*, Surface and Coatings Technology, 510 (2025) 132224.

<https://doi.org/10.1016/j.surfcoat.2025.132224>

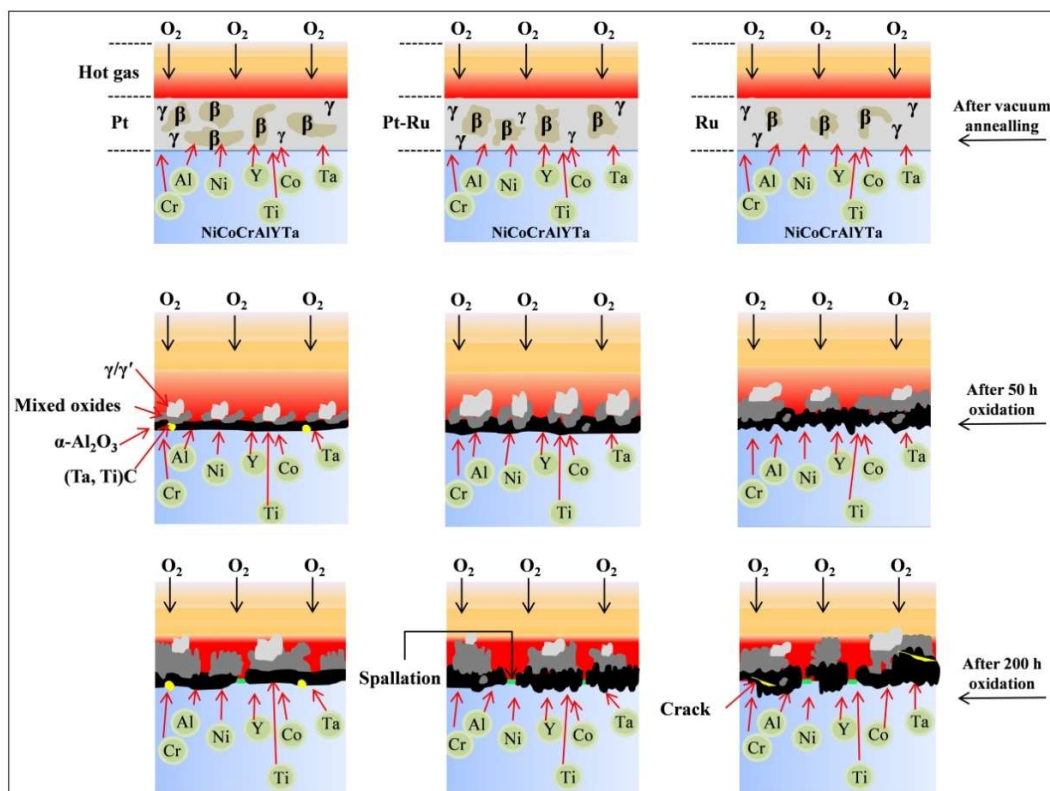


Figure 10. Mechanisms representing the oxidation evolution in the samples.

The role of Y, Ta, and Ti accommodation in the achieved microstructures further supports the enhancement observed in oxidation protection with increasing the Pt content. Y enhances adhesion and reduces the growth rate of the TGO layer [3, 66]. However, the enhanced accumulation of Y in the metallic islands with increasing the Ru content (Figures 6 and 7 and Table 4 and 5) negates its positive effect. Conversely, the reduced tendency of Y to diffuse into the islands with increasing the Pt content directs it toward the oxide layer, particularly the  $\text{Al}_2\text{O}_3$  layer, leading to its beneficial contribution. Additionally, as indicated in Tables 3 and 4 as well as Figures 7 and 9, with the increased Ru amount, Ta atoms accommodate within the metallic islands and mixed oxide zones, while Ti, which has a high oxidation tendency, tends to accommodate in the mixed oxide zones. In contrast, in the Pt-

**This is the accepted manuscript (postprint) of the following article:**

Majid Hosseinzadeh, Erfan Salahinejad, *Influence of Pt/Ru ratios on the oxidation mechanism of MCrAlYTa coatings modified with PtRu overlays*, Surface and Coatings Technology, 510 (2025) 132224.

<https://doi.org/10.1016/j.surfcoat.2025.132224>

coated sample, both Ti and Ta are expelled from the metallic islands, enabling the formation of (Ta, Ti)C in the oxide zones and minimizing the negative effect of Ti on oxidation protection. Additionally, the incorporation of Ta in the TGO layer of the Pt-coated sample enhances Al diffusivity [41, 67] while decreasing both the inward diffusion of oxygen [68] and the activity of  $O^{2-}$  [69], slowing the formation of  $Al_2O_3$ . As a result, the suppressed excessive growth of the TGO layer improves its adhesion and enhances oxidation resistance. The partitioning of these three elements (Ta, Y, and Ti) in the noted phases aligns well with the EDS results of the annealed samples (Table 3).

The existence of oxides other than alumina within the TGO layer of the Ru-coated samples is responsible for crack formation and spallation in the high Ru samples (Figures 6d and 8e), as can be elucidated via the Pilling–Bedworth ratio (PBR) and coefficient of thermal expansion (CTE) mismatch. PBR compares the volume of the oxide that forms to the volume of the metal consumed to form it. A PBR of 1.28 for  $Al_2O_3$  [70], as the dominant phase of the high Pt samples, is consistent with a protective oxide layer and desirable adhesion to the substrate. By increasing the Ru content of the overlays, and accordingly promoting the evolution of other oxides, primarily  $NiAl_2O_4$  (PBR  $\approx 2.62$  [71]), the oxide's volume significantly exceeds that of the original metal. As a result, during oxide formation, the oxide attempts to expand much more than the underlying metal can accommodate, while the metal substrate restricts this expansion. This mismatch generates substantial compressive stresses within the oxide layer, rendering it unstable and leading to spallation and cracking. On the other hand, the CTE values for  $NiCoCrAlYTa$ ,  $Al_2O_3$ , and  $NiAl_2O_4$  are  $18.4 \times 10^{-4}$  [72],  $8.5 \times 10^{-6}$  [73], and  $5.1 \times 10^{-6}$  [74]  $K^{-1}$ , respectively. The increase in CTE mismatch due to the formation of  $NiAl_2O_4$  in comparison to alumina further supports the observed cracking and spallation in

**This is the accepted manuscript (postprint) of the following article:**

Majid Hosseinzadeh, Erfan Salahinejad, *Influence of Pt/Ru ratios on the oxidation mechanism of MCrAlYTa coatings modified with PtRu overlays*, Surface and Coatings Technology, 510 (2025) 132224.  
<https://doi.org/10.1016/j.surfcoat.2025.132224>

the high Ru samples, as thermal cycling induces stress build-up, and upon heating and cooling, mismatch strains cause cracking, delamination, or spallation of the oxide layer.

## 5. Conclusions

This mechanistic study concluded that electrodeposited overlays within the Pt-Ru alloy system significantly enhance the high-temperature oxidation resistance of NiCoCrAlYTa bond coats in TBC systems. However, increasing the Ru content slightly reduces oxidation resistance due to the interplay of kinetic and thermodynamic interactions among the overlay, bond coat, and substrate elements. Nevertheless, given Ru's significantly lower cost compared to Pt, a comprehensive economic analysis, alongside durability evaluation, is essential to explore Ru as a lower-cost alternative or supplementary option to traditional Pt-modified coatings while maintaining or enhancing performance.

## References

1. Tolpygo, V.K. and D.R. Clarke, Surface rumpling of a (Ni, Pt)Al bond coat induced by cyclic oxidation. *Acta Materialia*, 2000. **48**(13): p. 3283-3293.
2. Birks, N., Introduction to the high temperature oxidation of metals. Cambridge Univ, 2006.
3. Padture, N.P., M. Gell, and E.H. Jordan, Thermal barrier coatings for gas-turbine engine applications. *Science*, 2002. **296**(5566): p. 280-284.
4. Oskay, C., M. Galetz, and H. Murakami, Oxide scale formation and microstructural degradation of conventional, Pt-and Pt/Ir-modified NiAl diffusion coatings during thermocyclic exposure at 1100° C. *Corrosion Science*, 2018. **144**: p. 313-327.
5. Yu, C., et al., High-temperature performance of Pt-modified Ni-20Co-28Cr-10Al-0.5 Y coating: Formation mechanism of Pt-rich overlayer and its effect on thermally grown oxide failure. *Surface and Coatings Technology*, 2023. **461**: p. 129422.
6. Gleeson, B., et al. Effects of platinum on the interdiffusion and oxidation behavior of Ni-Al-based alloys. in *Materials Science Forum*. 2004. Trans Tech Publ.
7. Put, A.V., et al., Effect of modification by Pt and manufacturing processes on the microstructure of two NiCoCrAlYTa bond coatings intended for thermal barrier system applications. *Surface and Coatings Technology*, 2010. **205**(3): p. 717-727.
8. Hou, P.Y., Impurity effects on alumina scale growth. *Journal of the American Ceramic Society*, 2003. **86**(4): p. 660-68.

**This is the accepted manuscript (postprint) of the following article:**

Majid Hosseinzadeh, Erfan Salahinejad, *Influence of Pt/Ru ratios on the oxidation mechanism of MCrAlYTa coatings modified with PtRu overlays*, Surface and Coatings Technology, 510 (2025) 132224.  
<https://doi.org/10.1016/j.surfcoat.2025.132224>

9. Pint, B., et al., Substrate and bond coat compositions: factors affecting alumina scale adhesion. *Materials Science and Engineering: A*, 1998. **245**(2): p. 201-211.
10. Sun, J., et al., Oxidation behaviour of Pt modified aluminized NiCrAlYSi coating on a Ni-based single crystal superalloy. *Corrosion Science*, 2018. **139**: p. 172-184.
11. Yang, S., et al., A novel single-phase  $\gamma'$  nanocrystalline coating with high resistance to oxidation and scale rumpling yet mitigated interdiffusion with the alloy substrate. *Corrosion Science*, 2021. **192**: p. 109866.
12. Khan, A., et al., Diffusion characteristics and structural stability of Pt modified  $\beta$ -NiAl/ $\gamma'$ -Ni<sub>3</sub>Al within NiCoCrAl alloy at high temperature. *Applied Surface Science*, 2019. **476**: p. 1096-1107.
13. Zhang, Y., et al., Effects of Pt incorporation on the isothermal oxidation behavior of chemical vapor deposition aluminide coatings. *Metallurgical and Materials Transactions A*, 2001. **32**: p. 1727-1741.
14. Tolpygo, V. and D. Clarke, Surface rumpling of a (Ni, Pt) Al bond coat induced by cyclic oxidation. *Acta materialia*, 2000. **48**(13): p. 3283-3293.
15. Mumm, D., A. Evans, and I. Spitsberg, Characterization of a cyclic displacement instability for a thermally grown oxide in a thermal barrier system. *Acta Materialia*, 2001. **49**(12): p. 2329-2340.
16. Tawancy, H., L.M. Alhems, and M. Aboelfotoh, Performance of Bond Coats Modified by Platinum Group Metals for Applications in Thermal Barrier Coatings. *Journal of Materials Engineering and Performance*, 2017. **26**: p. 3191-3203.
17. Zhao, Y., et al., Influence of Ru on high-temperature creep rupture properties and oxidation behavior of Ni-based single-crystal superalloys. *Materials Characterization*, 2024. **208**: p. 113620.
18. Yuan, K., et al. Influence of Ru, Mo and Ir on the Behavior of Ni-Based MCrAlY Coatings in High Temperature Oxidation. in *Turbo Expo: Power for Land, Sea, and Air*. 2014. American Society of Mechanical Engineers.
19. Vahlas, C., Microstructural characterization of Ru-doped NiCoCrAlYTa coupons treated by thermal oxidation. *Corrosion science*, 2009. **51**(9): p. 2192-2196.
20. Bai, B., et al., Cyclic oxidation and interdiffusion behavior of a NiAlDy/RuNiAl coating on a Ni-based single crystal superalloy. *Corrosion Science*, 2011. **53**(9): p. 2721-2727.
21. Karlsson, A.M. and A. Evans, A numerical model for the cyclic instability of thermally grown oxides in thermal barrier systems. *Acta Materialia*, 2001. **49**(10): p. 1793-1804.
22. Tryon, B., et al., Ruthenium-containing bond coats for thermal barrier coating systems. *JoM*, 2006. **58**: p. 53-59.
23. Hosseinzadeh, M. and E. Salahinejad, Comparative analysis of electrodeposited Pt, Ru and Pt-Ru overlays for high-temperature oxidation protection. *Surface and Coatings Technology*, 2025. **496**: p. 131685.
24. Okamoto, H. and T. Massalski, Thermodynamically improbable phase diagrams. *Journal of phase equilibria*, 1991. **12**: p. 148-168.
25. Kumar, A., et al., High performance CuO@ brass supercapacitor electrodes through surface activation. *Journal of Materials Chemistry A*, 2021. **9**(14): p. 9327-9336.
26. Garg, M., et al., High oxidation resistance of AlCoCrFeNi high entropy alloy through severe shear deformation processing. *Journal of Alloys and Compounds*, 2022. **917**: p. 165385.
27. Vande Put, A., et al., Influence of Pt Addition and Manufacturing Process on the Failure Mechanisms of NiCoCrAlYTa-Base Thermal Barrier Coating Systems under Thermal Cycling Conditions. *Metals*, 2018. **8**(10): p. 771.
28. Afanas'ev, V.P., et al., Comparative investigation of XPS spectra of oxidated carbon nanotubes and graphene. *Biophysica*, 2023. **3**(2): p. 307-317.
29. Vámos, C., et al., Analysis of time-dependent hydrophobic recovery on plasma-treated superhydrophobic polypropylene using XPS and wettability measurements. *Scientific Reports*, 2024. **14**(1): p. 23715.

**This is the accepted manuscript (postprint) of the following article:**

Majid Hosseinzadeh, Erfan Salahinejad, *Influence of Pt/Ru ratios on the oxidation mechanism of MCrAlYTa coatings modified with PtRu overlays*, Surface and Coatings Technology, 510 (2025) 132224.

<https://doi.org/10.1016/j.surfcoat.2025.132224>

30. Dwivedi, N., et al., Understanding the role of nitrogen in plasma-assisted surface modification of magnetic recording media with and without ultrathin carbon overcoats. Scientific reports, 2015. **5**(1): p. 7772.
31. Ahmadi, S., et al., XPS analysis and structural characterization of CZTS thin films deposited by one-step thermal evaporation. Journal of Alloys and Compounds, 2022. **925**: p. 166520.
32. Ghadami, F., A. Sabour Rouh Aghdam, and S. Ghadami, A comprehensive study on the microstructure evolution and oxidation resistance of conventional and nanocrystalline MCrAlY coatings. Scientific reports, 2021. **11**(1): p. 875.
33. Hierro-Oliva, M., A. Gallardo-Moreno, and M. González-Martín, XPS analysis of Ti6Al4V oxidation under UHV conditions. Metallurgical and Materials Transactions A, 2014. **45**: p. 6285-6290.
34. Wang, H.-C., et al., AlGaN/GaN MIS-HEMTs with high quality ALD-Al<sub>2</sub>O<sub>3</sub> gate dielectric using water and remote oxygen plasma as oxidants. IEEE Journal of the Electron Devices Society, 2017. **6**: p. 110-115.
35. Aitbekova, A., et al., Templated encapsulation of platinum-based catalysts promotes high-temperature stability to 1,100° C. Nature materials, 2022. **21**(11): p. 1290-1297.
36. Raja, J., et al., Improved data retention of InSnZnO nonvolatile memory by H<sub>2</sub>O<sub>2</sub> treated Al<sub>2</sub>O<sub>3</sub> tunneling layer: A cost-effective method. IEEE Electron Device Letters, 2016. **37**(10): p. 1272-1275.
37. Jin, Y., et al., Effect of Cr and W addition on the oxidation behavior of Ni–8% Al alloy at 1000° C. Vacuum, 2022. **200**: p. 111044.
38. Biesinger, M.C., et al., X-ray photoelectron spectroscopic chemical state quantification of mixed nickel metal, oxide and hydroxide systems. Surface and Interface Analysis: An International Journal devoted to the development and application of techniques for the analysis of surfaces, interfaces and thin films, 2009. **41**(4): p. 324-332.
39. Seal, S., S. Kuiry, and L. Bracho, Surface chemistry of oxide scale on IN-738LC superalloy: effect of long-term exposure in air at 1173 K. Oxidation of metals, 2002. **57**: p. 297-322.
40. Wang, Z., et al., XPS and ToF-SIMS investigation of native oxides and passive films formed on nickel alloys containing chromium and molybdenum. Journal of The Electrochemical Society, 2021. **168**(4): p. 041503.
41. Wang, H., et al., Effects of Ta and Y additions on the high temperature oxidation mechanisms of Ni–10Al alloy at 1100° C. Vacuum, 2023. **213**: p. 112074.
42. Qin, W., et al., Tribological properties of self-lubricating Ta-Cu films. Applied Surface Science, 2018. **435**: p. 1105-1113.
43. Qin, L., et al., Effect of Al<sub>2</sub>O<sub>3</sub> content on the high-temperature oxidation behaviour of CoCrAlYTa coatings produced by laser-induction hybrid cladding. Corrosion Science, 2022. **209**: p. 110739.
44. Simpson, R., et al., XPS investigation of monatomic and cluster argon ion sputtering of tantalum pentoxide. Applied Surface Science, 2017. **405**: p. 79-87.
45. Li, K., et al., Dry reforming of methane over La<sub>2</sub>O<sub>2</sub>CO<sub>3</sub>-modified Ni/Al<sub>2</sub>O<sub>3</sub> catalysts with moderate metal support interaction. Applied Catalysis B: Environmental, 2020. **264**: p. 118448.
46. Zhang, S., et al., Ni<sub>x</sub>Al<sub>1-x</sub>O<sub>2-δ</sub> mesoporous catalysts for dry reforming of methane: The special role of NiAl<sub>2</sub>O<sub>4</sub> spinel phase and its reaction mechanism. Applied Catalysis B: Environmental, 2021. **291**: p. 120074.
47. Bolt, P., et al., The interaction of thin NiO layers with single crystalline α-Al<sub>2</sub>O<sub>3</sub> (1120) substrates. Surface science, 1995. **329**(3): p. 227-240.
48. Wang, N., et al., Facile route for synthesizing ordered mesoporous Ni–Ce–Al oxide materials and their catalytic performance for methane dry reforming to hydrogen and syngas. Acs Catalysis, 2013. **3**(7): p. 1638-1651.
49. Tryon, B., et al., Hybrid intermetallic Ru/Pt-modified bond coatings for thermal barrier systems. Surface and Coatings Technology, 2007. **202**(2): p. 349-361.

**This is the accepted manuscript (postprint) of the following article:**

Majid Hosseinzadeh, Erfan Salahinejad, *Influence of Pt/Ru ratios on the oxidation mechanism of MCrAlYTa coatings modified with PtRu overlays*, Surface and Coatings Technology, 510 (2025) 132224.  
<https://doi.org/10.1016/j.surfcoat.2025.132224>

50. Li, W., et al., Improvement of cyclic oxidation resistance of a  $\beta$ -(Ni, Pt) Al coating by the addition of Ni/Ni-Re layer at 1150°C. *Corrosion Science*, 2022. **207**: p. 110486.
51. Ma, K. and J.M. Schoenung, Influence of cryomilling on the microstructural features in HVOF-sprayed NiCrAlY bond coats for thermal barrier coatings: creation of a homogeneous distribution of nanoscale dispersoids. *Philosophical Magazine Letters*, 2010. **90**(10): p. 739-751.
52. Ghadami, F., A.S.R. Aghdam, and S. Ghadami, Microstructural characteristics and oxidation behavior of the modified MCrAlX coatings: a critical review. *Vacuum*, 2021. **185**: p. 109980.
53. Li, Y., et al., Pt-modification on the thermal cycling behavior of NiCoCrAlYTa coating: A case study. *Corrosion Science*, 2024. **230**: p. 111934.
54. Tawancy, H., et al., Comparative performance of selected bond coats in advanced thermal barrier coating systems. *Journal of Materials Science*, 2000. **35**: p. 3615-3629.
55. Copland, E., Partial thermodynamic properties of  $\gamma'$ -(Ni, Pt) 3Al in the Ni-Al-Pt system. *Journal of Phase Equilibria and Diffusion*, 2007. **28**(1): p. 38-48.
56. Gaskell, D.R. and D.E. Laughlin, *Introduction to the Thermodynamics of Materials*. 2017: CRC press.
57. Wang, D., et al., NiAlHf/Ru: promising bond coat materials in thermal barrier coatings for advanced single crystal superalloys. *Corrosion science*, 2014. **78**: p. 304-312.
58. Chen, Y., et al., Effect of platinum addition on oxidation behaviour of  $\gamma/\gamma'$  nickel aluminide. *Acta Materialia*, 2015. **86**: p. 319-330.
59. Bellina, P., et al., Formation of discontinuous Al<sub>2</sub>O<sub>3</sub> layers during high-temperature oxidation of RuAl alloys. *Journal of Materials Research*, 2006. **21**(1): p. 276-286.
60. Mévrel, R., State of the art on high-temperature corrosion-resistant coatings. *Materials Science and Engineering: A*, 1989. **120**: p. 13-24.
61. Taylor, T.A. and D.F. Bettridge, Development of alloyed and dispersion-strengthened MCrAlY coatings. *Surface and Coatings Technology*, 1996. **86**: p. 9-14.
62. Hesnawi, A., et al., Isothermal oxidation behaviour of EB-PVD MCrAlY bond coat. *Vacuum*, 2007. **81**(8): p. 947-952.
63. Vjunitsky, I., et al., Study of phase states and oxidation of B2-structure based Al-Ni-Ru-M alloys. *Intermetallics*, 2005. **13**(1): p. 35-45.
64. Sun, J., et al., Microstructure and oxidation behaviour of Pt modified NiCrAlYSi coating on a Ni-based single crystal superalloy. *Surface and Coatings Technology*, 2020. **399**: p. 126164.
65. Tang, J., et al., Microstructural design and oxidation resistance of CoNiCrAlY alloy coatings in thermal barrier coating system. *Journal of Alloys and Compounds*, 2016. **688**: p. 729-741.
66. Wang, T., et al., Effect of Yttrium Additions on the High-Temperature Oxidation Behavior of GH4169 Ni-Based Superalloy. *Materials*, 2024. **17**(11): p. 2733.
67. Yang, L., et al., Diffusion of Ta and its influence on oxidation behavior of nanocrystalline coatings with different Ta, Y and Al contents. *Corrosion Science*, 2017. **126**: p. 344-355.
68. Gao, S., et al., Effects of Ta on the high temperature oxidation behavior of IN617 alloy in air. *Corrosion Science*, 2020. **170**: p. 108682.
69. Sato, A., Y.-L. Chiu, and R. Reed, Oxidation of nickel-based single-crystal superalloys for industrial gas turbine applications. *Acta Materialia*, 2011. **59**(1): p. 225-240.
70. Xu, C. and W. Gao, Pilling-Bedworth ratio for oxidation of alloys. *Material Research Innovations*, 2000. **3**: p. 231-235.
71. Li, C., et al., High-temperature oxidation and hot corrosion behavior of the Cr-modified aluminide coating obtained by a Thermal Diffusion process. *Materials Research Express*, 2019. **6**(8): p. 086444.
72. Feizabadi, A., et al., Cyclic oxidation characteristics of HVOF thermal-sprayed NiCoCrAlY and CoNiCrAlY coatings at 1000 °C. *Journal of Alloys and Compounds*, 2018. **746**: p. 509-519.

**This is the accepted manuscript (postprint) of the following article:**

Majid Hosseinzadeh, Erfan Salahinejad, *Influence of Pt/Ru ratios on the oxidation mechanism of MCrAlYTa coatings modified with PtRu overlays*, Surface and Coatings Technology, 510 (2025) 132224.

<https://doi.org/10.1016/j.surfcoat.2025.132224>

73. Wachtman Jr, J., T. Scuderi, and G. Cleek, Linear thermal expansion of aluminum oxide and thorium oxide from 100 to 1100 K. *Journal of the American Ceramic Society*, 1962. **45**(7): p. 319-323.
74. O'horo, M., A. Frisillo, and W. White, Lattice vibrations of MgAl<sub>2</sub>O<sub>4</sub> spinel. *Journal of Physics and Chemistry of Solids*, 1973. **34**(1): p. 23-28.